

Orbital excitations in LaMnO₃

Jeroen van den Brink

*Computational Materials Science and Mesa⁺ Institute, Faculty of Applied Physics,
University of Twente, P.O. Box 217, 7500 AE Enschede, The Netherlands*

(November 6, 2018)

We study the recently observed orbital excitations, orbitons, and treat electron-electron correlations and lattice dynamics on equal footing. It is shown that the orbiton energy and dispersion are determined by both correlations and lattice-vibrations. The electron-phonon coupling causes satellite structures in the orbiton spectral function and the elementary excitations of the system are mixed modes with both orbital and phonon character. It is proposed that the satellite structures observed in recent Raman-scattering experiments on LaMnO₃ are actually orbiton derived satellites in the phonon spectral function, caused by the phonon-orbiton interaction.

Elementary properties of electrons in atoms and solids are determined by their charge and spin, but in many correlated electron materials also by their orbital degree of freedom [1,2]. In a free transition metal atom, with an open d shell, the $3d$ energy levels are five-fold orbitally degenerate, where each orbital state corresponds to a different quadrupolar charge-distribution in real-space. In correlated Mott-insulators, among which there are many transition metal oxides (TMO's), monopolar charge excitations, that involve moving charge from one atom to another, are only possible at high energies because of the large Coulomb interaction between electrons. However, low energy multipolar charge excitations -corresponding to orbital excitations- are possible as they can be locally charge-neutral.

In a solid the orbital degeneracy of a free ion is lifted. There are two physically distinct mechanisms. One possibility is that the electron-electron interaction splits the states via the superexchange and in this way couples orbitals to the spin and relates orbital- to magnetic-order [2]. On the other hand, also the electron-phonon interaction, which gives rise to orbital order accompanied by a Jahn-Teller lattice distortion [3], can lift the degeneracy. The resulting orbital order is found in many TMO's, ranging from titanates (e.g. YTiO₃ [4]), vanadates (e.g. V₂O₃ [5], LiVO₂ [6], YVO₃ [7]) and manganites (e.g. LaMnO₃ [8], Nd_{1/2}Sr_{1/2}MnO₃ [9]), to cuprates (e.g. KCuF₃ [2]). The quadrupolar charge ordering -orbital ordering- should give rise to elementary excitations with orbital signature, as the order causes a breaking of symmetry in the orbital sector. The existence of such excitations, orbitons, was predicted in the 70's and theoretically studied ever since [2,10-12], but only very recently orbitons were observed for the first time in a Raman scattering experiment on LaMnO₃ [13]. The observed orbitons were interpreted by some as being due to electron correlations [13], but others suggest that they originate from the electron-lattice coupling [14]. This motivates us to address the question of the origin of the orbitons, also because it is important to establish the

precise nature of the orbitons as they, in turn, have a large effect on spin [15,16] and monopolar charge excitations [17,18].

We use a realistic model Hamiltonian for LaMnO₃ that incorporates both superexchange and electron-phonon coupling. We study the Hamiltonian first in the localized limit in order to gain more physical insight into the problem. This approach illustrates that for groundstate properties it is usually sufficient to treat the Jahn-Teller phonons as classical entities [19], but that for orbital dynamics it is essential to treat the lattice-vibrations quantum-mechanically. The full calculation shows that in LaMnO₃ the orbiton has exchange and lattice character: its energy and dispersion are determined by both correlations and phonons. We propose that the peaks in the Raman-scattering data on LaMnO₃ [13], are orbiton derived satellites in the phonon spectral function, which arise due to the mixing of the orbital and phonon modes.

Hamiltonian. We consider the two-fold degenerate manganese e_g states, with one electron per site. The electron can either be in the $x^2 - y^2$ or $3z^2 - r^2$ orbital, or in any linear combination of these two states. The interaction between neighboring orbitals is mediated by the superexchange and the electron-phonon (e-p) interaction couples the electron to the two-fold degenerate Jahn-Teller phonons that have e_g symmetry. We also take into account the dispersion of these phonons. Let us split up the Hamiltonian in an orbital, e-p and free phonon part: $H = H_{orb} + H_{ep} + H_{ph}$, with

$$H_{orb}^0 + H_{e-p}^0 = \sum_{\langle ij \rangle \Gamma} J_{\Gamma} T_i^{\Gamma} T_j^{\Gamma} + 2g \sum_i \tau_i^z Q_{3i} + \tau_i^x Q_{2i}, \quad (1)$$

where the sum is over neighboring sites $\langle ij \rangle$ along the $\Gamma = a, b, c$ crystallographic axes. The orbital operators T_i^{Γ} can be expressed in terms of the Pauli matrices τ : $T_i^{a/b} = (\tau_i^z \pm \sqrt{3}\tau_i^x)/2$, and $T_i^c = \tau_i^z$. The e-p coupling constant is denoted by g and the phonon operators of the so-called Q_2 and Q_3 Jahn-Teller modes with e_g symmetry are $Q_{2/3i} = q_{2/3i}^{\dagger} + q_{2/3i}$. The free phonon part of the Hamiltonian is then

$$H_{ph}^0 = \omega_0 \sum_i \left[q_{3i}^\dagger q_{3i} + q_{2i}^\dagger q_{2i} \right] + \omega_1 \sum_{\langle ij \rangle r} Q_i^\Gamma Q_j^\Gamma, \quad (2)$$

where the local phonon energy is given by ω_0 and the nearest neighbor coupling between the phonons by ω_1 . The coupled Jahn-Teller modes along the three spatial axes are $Q_i^{a/b} = (Q_{3i} \pm \sqrt{3}Q_{2i})/2$ and $Q_i^c = Q_{3i}$ [20]. Note that the orbital excitations are locally charge neutral and do therefore not couple to breathing mode distortions.

The Hamiltonian Eqs.(1,2) is general and one needs to make it more specific in order to describe LaMnO₃. This is a prototype of an orbital ordered and Jahn-Teller distorted system and its crystallographic structure basically consists of corner connected MnO₆ octahedra, where the space between octahedra is filled with Lanthanum atoms. Due to the correlation and Jahn-Teller coupling the octahedra are elongated, with the axis of elongation along the crystallographic a -direction on one sublattice, and along the b -direction on the other, such that the reciprocal lattice vector for the orbital order is $\mathbf{Q} = (\pi, \pi, 0)$. An intersite phonon coupling arises because the elongation of a MnO₆ octahedron induces a contraction of the neighboring octahedron, and vice versa, as the octahedra have one corner in common. The orbital order is formally incorporated in the Hamiltonian by performing a rotation of the T operators [11], with equal orbital exchange constants $J_a = J_b = J$ along the two axes in the plane.

Transformations. In analogy with linear spin wave theory, the orbital modes can be found by performing a Holstein-Primakov transformation [11]. We introduce on each site i the bosonic orbital operators q_{1i}^\dagger and q_{1i} : $\tau_i^z = \frac{1}{2} - q_{1i}^\dagger q_{1i}$ and $\tau_i^x = \frac{1}{2}(q_{1i}^\dagger + q_{1i})$. We see from Eq. (3) that this transformation introduces a term that is linear in the phonon mode Q_3 in H_{e-p} . This is a consequence of the long range orbital order that we assumed to be present from the beginning: the lattice deforms according to the symmetry of the occupied orbital on each site. The linear term can be gauged away by introducing $q_3 \rightarrow q_3 + \eta$, where the shift η is given by $\eta = g/(\omega_0 - 6\omega_1)$. After this shift we collect the quadratic and cubic terms in the bosonic operators and find in Fourier space

$$H_{orb} = \sum_k (3J + 4g\eta) q_{1k}^\dagger q_{1k} - \frac{J\gamma_{1k}}{4} Q_{1k} Q_{1-k} \quad (3)$$

$$H_{e-p} = g \sum_{k,q} 2 q_{1k-q}^\dagger q_{1k} Q_{3q} + Q_{1k} Q_{2-k} \quad (4)$$

$$H_{ph} = \omega_0 \sum_k \left[q_{3k}^\dagger q_{3k} + q_{2k}^\dagger q_{2k} + \frac{\omega_1}{2} (\gamma_{2k} Q_{2k} Q_{2-k} - 3\gamma_{\parallel k} Q_{3k} Q_{3-k}) \right], \quad (5)$$

with $Q_{\nu k} = q_{\nu k}^\dagger + q_{\nu -k}$ and the dispersions $\gamma_{1k} = \gamma_{\parallel k} + \gamma_{\perp k} J_c/J$, $\gamma_{2k} = 2\gamma_{\perp k} - \gamma_{\parallel k}$, where $\gamma_{\parallel k} = (\cos k_x + \cos k_y)/2$ and $\gamma_{\perp k} = \cos k_z$ [21].

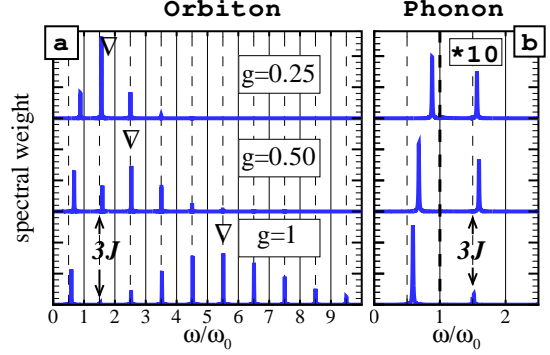


FIG. 1. (a) Orbiton (Q_1) and (b) phonon (Q_2) spectral function in the localized limit. The first pole due to the orbital exchange is indicated at $3J$. In the orbital spectrum the static crystal-field energy \bar{J} is indicated by ∇ . The spectral weight in (b) is multiplied by 10 for $\omega > \omega_0$.

Three important consequences of the orbiton-phonon coupling are present in Eqs. (3-5). First, the coupling to the lattice moves the orbiton to higher energy an amount $4g\eta$. This shift has a straightforward physical meaning: it is phonon contribution to the crystal-field splitting of the e_g states caused by the static Jahn-Teller lattice deformation [22]. If, however, an orbital excitation is made, it strongly interacts with the Q_3 phonon (Eq. 4), so that the orbital excitation can be dynamically screened by the Jahn-Teller phonons and lowered in energy. The crystal-field splitting and screening are strongly competing as both are both governed by the energy scale set by the e-p coupling. Finally, the orbital and Q_2 phonon modes mix, as is clear from the second term of H_{e-p} . This implies that the true eigenmodes of the coupled orbital-phonon system have both orbital and phonon character.

Localized limit. We illustrate the three physical effects of the orbiton-phonon coupling, discussed above, by considering the Hamiltonian of Eqs. (3-5) first in the localized limit, neglecting all dispersion. The Hamiltonian then reduces to

$$H_{loc} = (\bar{J} + 2gQ_3) q_1^\dagger q_1 + \omega_0 (q_3^\dagger q_3 + q_2^\dagger q_2) + gQ_1 Q_2, \quad (6)$$

with $\bar{J} = 3J + 4g\eta$, which is the sum of the local orbital exchange energy and static phonon contribution to the crystal-field splitting. The Hamiltonian without the last term is exactly solvable by a canonical transformation [23] so that we can obtain the expressions for the 6 by 6 matrix of bosonic Green's functions $D_{11}(\nu, t - t') = -i\langle\langle T q_\nu^\dagger(t) q_\nu(t') \rangle\rangle$, $D_{12}(\nu, t - t') = -i\langle\langle T q_\nu(t) q_\nu(t') \rangle\rangle$, $D_{21}(\nu, t - t') = -i\langle\langle T q_\nu^\dagger(t) q_\nu^\dagger(t') \rangle\rangle$, $D_{22}(\nu, t - t') = -i\langle\langle T q_\nu(t) q_\nu^\dagger(t') \rangle\rangle$, with $\nu = 1, 2, 3$. The last term in Eq. (6) couples the orbiton and Q_2 phonon mode and introduces a self energy [24]. We use the on-site Jahn-Teller vibrational energy $\omega_0 = 80$ meV as unit of energy, and $J = \omega_0/2$, in accordance with Refs. [13,17]. In Fig. 1a the calculated orbiton spectral function, $-\frac{1}{\pi} \text{Im} D(1, \omega)$, is plotted. For small e-p coupling g , most of the spectral weight is in the pole at

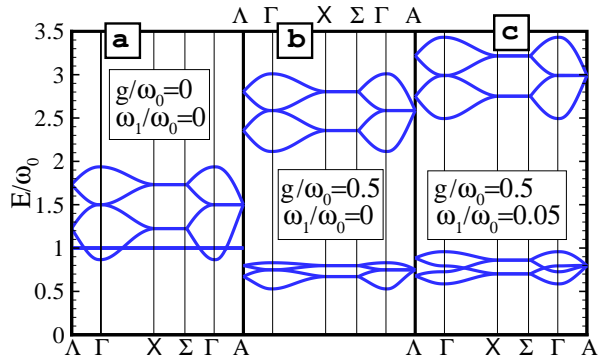


FIG. 2. Orbital and phonon dispersion, neglecting dynamical effects due to the e-p coupling; (a) without e-p coupling g and without bare phonon dispersion, (b) $g/\omega_0 = 1/2$, no bare phonon dispersion, and (c) $g/\omega_0 = 1/2$, finite bare phonon dispersion. The points of high symmetry in the Brillouin zone correspond to those of Ref. [13].

$\omega \approx 3J$, and phonon satellites with decreasing intensity are present at higher frequencies, at energy intervals ω_0 . The satellites are also known as Frank-Condon sidebands [12], and their weight increases with increasing e-p coupling strength. For larger coupling constants the *average* orbital excitation energy increases, caused by the increase of the crystal-field splitting, but low and high energy satellites are always present due to the interaction of the orbital excitation with lattice vibrations.

The mixing of orbital and phonon mode gives rise to one extra phonon satellite in the orbital spectral function, at frequencies below ω_0 . In Fig. 1b we see that, vice versa, due to the mixing a low intensity orbital satellite at $\approx 3J$ is present in the Q_2 phonon spectral function. The Q_2 vibrational mode softens with increasing g , in contrast to the the Q_3 mode, which is not affected by the e-p interaction.

Full Hamiltonian. The quadratic parts of the Hamiltonian in Eqs.(3-5) can be diagonalized by a generalized Bogoliubov transformation. For the moment we do not consider the cubic terms, that give rise to the dynamical screening of the orbital excitation. In the transformed operators the Hamiltonian is $H_{quad} = \sum_{\nu k} \epsilon_{\nu k} \alpha_{\nu k}^\dagger \alpha_{\nu k}$, with $q_{\nu k}^\dagger = \sum_{\mu} u_{\nu\mu}^k \alpha_{\mu k}^\dagger + v_{\nu\mu}^k \alpha_{\mu-k}$. The energies of the eigenstates are given by

$$\begin{aligned} \epsilon_{1,2k}^2 &= \zeta_k + \chi_k \pm [(\zeta_k - \chi_k)^2 + 4g^2 \bar{J} \omega_0]^{\frac{1}{2}} \\ \epsilon_{3k}^2 &= \omega_0(\omega_0 - 6\gamma_{\parallel k} \omega_1), \end{aligned} \quad (7)$$

with $\zeta_k = \bar{J}(\bar{J} - \gamma_{1k})/2$ and $\chi_k = \omega_0(\omega_0 + 2\gamma_{2k} \omega_1)/2$. The analytical expressions for $u_{\nu\mu}^k$ and $v_{\nu\mu}^k$ are rather involved. In Fig. 2 the dispersion of the eigenmodes ϵ_{1k} and ϵ_{2k} are shown for different sets of parameters, where we used $J_c/J = 0.5$ [13]. The modes with predominantly phonon character are centered around $E \approx \omega_0$, and with orbital character around the crystal-field energy \bar{J} . For the parameters indicated in of Fig. 2b the wavefunctions

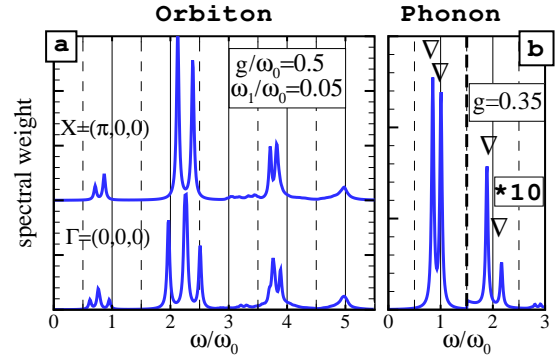


FIG. 3. (a) Orbital spectral function at the Γ and X-point, $g = \omega_0/2$. (b) Spectrum of the Raman-active A_g and B_{1g} phonon modes for $\omega_1/\omega_0 = 0.05$ and $g/\omega_0 = 0.35$. The experimental peak positions are indicated by ∇ . For $\omega > \omega_0$ the spectral weight is multiplied by 10, $g = 0.35\omega_0$, $\omega_1/\omega_0 = 0.05$.

of the low energy excitations have on average 95% phonon character and the high energy modes 95% orbital character. Note that the orbital dispersion is almost entirely due to the exchange coupling J and that via the e-p coupling the orbital dispersion reflects itself in the effective phonon dispersion.

We now consider the interaction between the eigenmodes via the cubic term in Eq.(4). The cubic terms can be taken into account in a diagrammatic expansion. The first non-zero diagram corresponds to an orbital that excites a phonon, propagates and absorbs the phonon again, which is a second order process. We calculate the self-energy due to this process self-consistently, i.e. instead of the bare orbital propagator, we use the orbital propagator dressed with phonon excitations. This is equivalent to the self-consistent Born approximation, as is used, for instance, to calculate properties of a single hole in the t-J like models [17,25]. This approximation works exceptionally well in t-J like models, for the problem of a single hole that is strongly coupled to magnons, or phonons [26], giving us confidence in its accuracy for the problem of a single orbital excitation coupled to phonons, which we consider here.

After the Bogoliubov transformation, the single cubic term in Eq.(4) maps into eight different non-zero cubic combinations of the new $\alpha_{\nu k}$ operators. We can make use of the observation that, in the parameter regime that we consider, the eigenmodes $\epsilon_{1,2k}$ have almost entirely orbital c.q. phonon character. The calculated self-energy is therefore dominated by only one of the eight cubic combinations of $\alpha_{\nu k}$ operators, which is at least an order of magnitude larger than other terms. Physically, this term is due to the orbital-phonon scattering process described in the previous paragraph. Details of the derivation will be published elsewhere [24].

The self-consistent calculation is performed numerically, taking about 10^4 points in the Brillouin-zone and an energy-grid with meshsize $\omega_0/100$. The resulting or-

biton spectral function at two high symmetry points in the Brillouin zone is shown in Fig. 3a, where we used the same parameters as in Fig. 2c. Comparing these two figures, we see that due to the dynamical e-p coupling the poles with mainly orbital character are shifted to lower frequency and that at higher frequency phonon induced satellites develop. This is not unexpected, as the same happens for the system in the localized limit (see Fig. 1a). A closer look to the orbital spectrum at the Γ -point, however, reveals also that the effective *orbital dispersion* is $\omega_0/2$, whereas the free orbital dispersion is ω_0 . The reduced dispersion can be understood as a consequence of polaronic band-narrowing: the effective mass of the orbital excitation increases because of its dressing with phonons.

Finally we can compare the calculated spectral function of the Raman-active A_g and B_{1g} phonon modes, shown in Fig. 3b, with experiment [13]. The main phonon lines below ω_0 and the weak orbiton induced satellites at $\approx 2\omega_0$ are in excellent agreement with experiment. The orbiton satellites are, just as in the localized limit (see Fig. 1b), due to the mixing of orbital and phonon modes. The value of the e-p coupling that is used in the phonon calculation, $g/\omega_0 = 0.35$, corresponds to rather weak electron-phonon coupling, in accordance with Ref. [27], but in contrast to Ref. [12]. If we were to use a larger value of g , the orbiton dispersion would become too small. A way to determine the e-p coupling regime experimentally is to check for additional satellites in the Raman spectrum at about $\omega \approx 3\omega_0$, which for the coupling strength in the present calculation have low intensity, but would have large intensity if the system were in the strong coupling regime [12]. It is crucial that we took the phonon-dynamics into account, as a purely static Jahn-Teller distortion (as in Ref. [13], see also Fig. 2c) would lead to an orbital dispersion that is about a factor two too large. We interpret the Raman peaks around 150 meV as orbiton satellites of the phonon peaks around 80 meV, which would disappear without electron-phonon coupling. This is in contrast to Saitoh et al. [13], where the peaks are due to different Raman scattering mechanisms and are assumed to be independent, which implies strong dependence of their intensity ratios on incident photon energy.

Conclusions. We calculated the orbiton and phonon properties for a realistic model Hamiltonian for LaMnO_3 and compare the results with Raman-scattering data. We treat electron-electron correlations and lattice dynamics on equal footing and have shown that the orbiton dispersion, which is mainly caused by correlation effects, is strongly reduced by the electron-phonon coupling. This coupling also mixes the orbiton and phonon modes and causes satellite structures in the orbiton and phonon spectral function. The elementary excitations of the system, in other words, are mixed modes with both orbital and phonon character. This leads us to interpret

the features around 150 meV in recent Raman-scattering experiments on LaMnO_3 as orbiton derived satellites in the phonon spectral function. These satellites should also be observable in other experiments that probe phonon dynamics, for instance in neutron scattering.

-
- [1] M. Imada, A. Fujimori and Y. Tokura, Rev. Mod. Phys. **70**, 1039 (1998), Y. Tokura, N. Nagaosa, Science **288**, 462 (2000).
 - [2] K. I. Kugel and D. I. Khomskii, Sov. Phys. JETP **37**, 725 (1973); Sov. Phys.-Usp. **25**, 232 (1982).
 - [3] H. A. Jahn and E. Teller, Proc. R. Soc. **A161**, 220 (1937).
 - [4] H. Ichikawa *et al.*, Physica B **281**, 482 (2000), H. Sawada and K. Terakura, Phys. Rev. B. **58**, 6831 (1998).
 - [5] C. Castellani, C. R. Natoli and J. Ranninger, Phys. Rev. B. **18**, 4945 (1978).
 - [6] H.F. Pen *et al.*, Phys. Rev. Lett. **78**, 1323 (1997).
 - [7] Y. Ren *et al.*, Nature **396**, 441 (1998).
 - [8] J. B. Goodenough, *Magnetism and Chemical Bond* (Interscience, New York, 1963).
 - [9] H. Kuwahara *et al.*, Science **270**, 961 (1995).
 - [10] S. Ishihara and J. Inoue, Phys. Rev. B **55**, 8280 (1997).
 - [11] J. van den Brink *et al.*, Phys. Rev. B **59**, 6795 (1999).
 - [12] P.B. Allen and V. Perebeinos, Phys. Rev. Lett. **83**, 4828 (1999).
 - [13] E. Saitoh *et al.*, Nature **410**, 180 (2001).
 - [14] P.B. Allen and V. Perebeinos, Nature **410**, 155 (2001).
 - [15] L. F. Feiner, A. M. Oles, and J. Zaanen Phys. Rev. Lett. **78**, 2799-2802 (1997).
 - [16] J. van den Brink *et al.*, Phys. Rev. B **58**, 10276 (1998).
 - [17] J. van den Brink, P. Horsch and A.M. Oles Phys. Rev. Lett. **85**, 5174 (2000), W.G. Yin, H.Q. Lin and C.D. Gong, Phys. Rev. Lett. **87**, 047204 (2001).
 - [18] V. Perebeinos and P.B. Allen, Phys. Rev. Lett. **85**, 5178 (2000).
 - [19] T. Hotta *et al.*, Phys. Rev. B **60** R15009 (1999).
 - [20] G. Khaliullin and R. Kilian, Phys. Rev. B **61**, 3494 (2000).
 - [21] Note that the 'mixed terms' in H_{orb} , containing products $\tau^x \tau^z$, are neglected. This is a reasonable approximation [11,17]. This also holds for terms of the same symmetry in H_{ph} .
 - [22] J. Bala and A.M. Oles, Phys. Rev. B **62**, R6085 (2000).
 - [23] See, for instance, G.D. Mahan, Many-Particle Physics, Plenum, New York (1990).
 - [24] J. van den Brink, to be published.
 - [25] C. L. Kane, P. A. Lee and N. Read, Phys. Rev. B **39**, 6880 (1989), G. Martínez and P. Horsch, Phys. Rev. B **44**, 317 (1991).
 - [26] A. Ramsak, P. Horsch and P. Fulde, Phys. Rev. B **46**, 14305 (1992).
 - [27] P. Benedetti and R. Zeyher, Phys. Rev. B **59**, 9923 (1999).